HHS Public Access

Author manuscript

FEBS Lett. Author manuscript; available in PMC 2019 September 01.

Published in final edited form as:

FEBS Lett. 2018 September ; 592(18): 3101–3110. doi:10.1002/1873-3468.13221.

Consequences of Cre-Mediated Deletion of *Ciz1* Exon 5 in Mice

Jianfeng Xiao[1], **Mohammad Moshahid Khan**[1], **Satya Vemula**[1], **Jun Tian**[1,2], and **Mark S. LeDoux**[1,*]

[1]Departments of Neurology, and Anatomy and Neurobiology, University of Tennessee Health Science Center, Memphis, TN, 38163, USA

[2]Department of Neurology, Second Affiliated Hospital, School of Medicine, Zhejiang University, Hangzhou, Zhejiang, 310009, P.R. China

Abstract

CIZ1 plays a role in DNA synthesis at the G1/S checkpoint. *Ciz1* gene-trap null mice manifest motor dysfunction, cell-cycle abnormalities and DNA damage. In contrast, it has previously been reported that mouse embryonic fibroblasts derived from presumed *Ciz1* knock-out mice (*Ciz1* $^{tm1.1Homy/tm1.1Homy}$) generated by crossing Cre-expressing mice with exon 5-floxed mice (*Ciz1* $^{tm1Homy/tm1Homy}$) do not exhibit evidence of enhanced DNA damage following γ-irradiation or cell-cycle defects. Here, we report that *Ciz1* $^{tm1.1Homy/tm1.1Homy}$ mice show loss of *Ciz1* exon 5 but are neurologically normal and express abnormal transcripts (*Ciz1*$^{\Delta E5/\Delta E5}$ mice) that are translated into one or more proteins of approximate wild-type size. Therefore, *Ciz1* $^{tm1.1Homy/tm1.1Homy}$ mice (*Ciz1*$^{\Delta E5/\Delta E5}$) lose residues encoded by exon 5 but may gain function from novel amino acid sequences.

Keywords

CIZ1; RNA-Seq; cerebellum; floxed; dystonia

CIZ1, a cell-cycle protein highly expressed in brain, is involved in DNA synthesis and localization of Xist RNA to the inactive X-chromosome (Mitsui et al., 1999, Coverley et al., 2005, Ridings-Figueroa et al., 2017). Depletion of *Ciz1* transcripts suppresses S phase entry. CIZ1 interacts with CDK2, cyclin E, cyclin A and p21 (Copeland et al., 2010, Mitsui et al., 1999), attaches to the nuclear matrix, and may contribute to the spatial organization of DNA replication (Ainscough et al., 2007). CIZ1 appears to play a role in dystonia, Alzheimer disease and several types of cancer (Yin et al., 2013, Warder and Keherly, 2003, Nishibe et al., 2013, Liu et al., 2015, Wu et al., 2015, Judex et al., 2003). In particular, co-segregating disease-causing missense variants were found in a family with cervical dystonia (Xiao et al., 2012), and altered splicing in exon 8 of *CIZ1* was found to be associated with Alzheimer

*Corresponding author, University of Tennessee Health Science Center, Department of Neurology, 855 Monroe Avenue, Suite 415 Link Building, Memphis, TN, 38163, USA, Telephone: 901-448-1662, mledoux@uthsc.edu.

Author contributions

JX, MMK, and MSL conceived and designed the experiments and analyzed the data; JX, MMK and JT performed the experiments; SV analyzed RNA_Seq data; JX and MSL wrote the paper.

disease (Dahmcke et al., 2008). A CIZ1 variant is a circulating biomarker of early-stage lung cancer (Higgins et al., 2012b).

To understand the neural function of CIZ1, particularly in post-mitotic neurons, we generated and phenotypically characterized a *Ciz1* gene-trap knock-out (KO, $Ciz1^{-/-}$) mouse model (Xiao et al., 2016a, Khan et al., 2018). $Ciz1^{-/-}$ mice manifest motor, behavioral and cognitive abnormalities that progress with age (Xiao et al., 2016a, Khan et al., 2018). The brains of aged (18-month-old) $Ciz1^{-/-}$ mice show evidence of overt DNA damage, NF-kB upregulation, oxidative stress, vascular dysfunction, inflammation, and cell death. Moreover, $Ciz1^{-/-}$ mouse embryonic fibroblasts (MEFs) were found to be abnormally sensitive to γ-irradiation. In contrast to our findings, presumed KO mice ($Ciz1^{tm1.1Homy/tm1.1Homy}$) generated with the Cre/loxP system had no reported motor or behavior phenotype, and MEFs from these mice showed no evidence of cell-cycle dysfunction or defects in the DNA damage response (Nishibe et al., 2013). To better address reported differences between these two lines of mice and explore the possibility of spatial and temporal control of CIZ1 expression, $Ciz1^{+/tm1Homy}$ mice were acquired from RIKEN BioResource Research Center (Tsukuba, Ibaraki, Japan, http://www2.brc.riken.jp), bred and crossed to Cre deleter mice. Herein, we show that crossing $Ciz1^{tm1Homy/tm1Homy}$ mice to Cre deleter mice eliminated a floxed exon 5 but did not prevent expression of alternative transcripts with sequences derived from introns 4 and 5 ($Ciz1^{\Delta E5/\Delta E5}$ mice). $Ciz1^{\Delta E5/\Delta E5}$ mice were examined with a battery of motor tests and their MEFs were examined for evidence of cell cycle abnormalities and defects in the DNA damage response.

Materials and methods

Mice

All mouse experiments were performed in accordance with the National Institutes of Health's Guidelines for the Care and Use of Laboratory Animals and approved by our Institutional Animal Care and Use Committee. Four adult heterozygous mice ($Ciz1^{+/tm1Homy}$, 2 males and 2 females) were purchased from the RIKEN BioResource Research Center (RBRC05198) (B6;129P2-*Ciz1*<tm1Homy>*Ciz1*]. These *Ciz1*-floxed mice were developed by Hiroaki Honda, Research Institute for Radiation Biology and Medicine, Hiroshima University in 2008 (Nishibe et al., 2013). In brief, a loxP site was inserted upstream of exon 5 and an FRT-flanked neo cassette with a 3' loxP site was inserted downstream of exon 5. The neo cassette was removed by crossing with FLPe mice [C57BL/6-Tg(CAG-FLPe)36Ito]. Heterozygous mice were backcrossed with C57BL/6NCrlCrlj mice at the RBRC for at least 6 generations prior to shipment. After receipt at the University of Tennessee Health Science Center, the $Ciz1^{+/tm1Homy}$ mice were backcrossed to C57BL/6J mice for at least 6 generations. Exon 5 was removed by crossing $Ciz1^{+/tm1Homy}$ mice with B6.Cg-Tg(Sox2-cre)1Amc/J mice purchased from the Jackson Laboratory (www.jax.org) to generate $Ciz1^{+/tm1.1Homy}$ and $Ciz1^{tm1.1Homy/tm1.1Homy}$ mice (herein referred to as $Ciz1^{+/\Delta E5}$ and $Ciz1^{\Delta E5/\Delta E5}$). To confirm results, $Ciz1^{+/tm1Homy}$ mice were also crossed with Hs-cre1 mice (Dietrich et al., 2000) to generate $Ciz1^{+/\Delta E5}$ and $Ciz1^{\Delta E5/\Delta E5}$ mice. The PCR genotyping protocol for $Ciz1^{+/tm1Homy}$ and $Ciz1^{+/tm1.1Homy}$ mice is provided by RBRC (www2.brc.riken.jp/animal/pdf/05198_PCR.pdf).

Ciz1 expression

Relative levels of mouse *Ciz1* mRNA were determined in 6 brain regions (cerebral cortex, cerebellum, hippocampus, striatum, thalamus, and mid brain), cervical spinal cord, and liver harvested from 3 adult male mice (3-month-old) of each genotype (*Ciz1*$^{+/+}$, *Ciz1*$^{tm1Homy/tm1Homy}$ [*Ciz1*$^{flox/flox}$], and *Ciz1*$^{\Delta E5/\Delta E5}$). TaqMan-based relative quantitative real-time reverse transcription PCR (QRT-PCR) was performed using two primer pairs and probes (Table S1) with a LightCycler® 480 System (Roche, Indianapolis, IN, USA). Mouse β-actin was used as an endogenous control. Detailed methods are provided in previous work from our laboratory (Xiao et al., 2016a).

For RNA-sequencing (RNA-Seq), total RNA from mouse cerebellum was isolated from one adult (3 month-old) male *Ciz1*$^{\Delta E5/\Delta E5}$ mouse and one age and gender matched *Ciz1*$^{+/+}$ sibling (Ambion™ TRI Reagent®, ThermoFisher Scientific, Waltham, MA, USA). After DNAse treatment (DNA-*free*™ DNA Removal Kit, ThermoFisher Scientific) the quality of total RNA was assessed with a NanoDrop® ND-1000 spectrophotometer (NanoDrop Technologies) and RNA integrity was verified with an Agilent 2100 Bioanalyzer using the Agilent RNA 6000 Nano kit. RNA was quantified with a Qubit 2.0 fluorometer (Life Technologies, Carlsbad, CA, USA). RNA library preparation and sequencing was performed by GENEWIZ (South Plainfield, NJ, USA). RNA samples were retreated with ThermoFisher TURBO DNase. RNA sequencing library preparations used the NEBNext Ultra RNA Library Prep Kit (NEB, Ipswich, MA, USA). Briefly, mRNA was enriched with oligo(dT) beads and fragmented for 15 min at 94°C. First and second strand cDNA were synthesized and cDNA fragments were end repaired and 3'-adenylated prior to ligation of universal adapters, index addition and library enrichment. The sequencing libraries were assessed with the Agilent TapeStation and quantified with a Qubit 2.0 fluorometer. The libraries from the *Ciz1*$^{+/+}$ and *Ciz1*$^{\Delta E5/\Delta E5}$ mice were loaded onto one lane of an Illumina (San Diego, CA, USA) HiSeq. The samples were sequenced using a 2×150 paired-end configuration. Image analysis and base calling were conducted by the HiSeq control software. Raw sequence data (binary base call [BCL] format) generated from Illumina HiSeq was converted into fastq files and de-multiplexed using Illumina's bcl2fastq 2.17 software. One mismatch was allowed for index sequence identification.

Pre-alignment quality control (QC), alignment, and differential expression were analyzed with Partek Flow and Partek Genomic Suite (St. Louis, MO, USA). Reads were aligned to the Mouse Dec. 2011 (GRCm38/mm10) assembly using Spliced Transcripts Alignment to a Reference (STAR) and quantified to RefSeq transcripts using the Partek expectation-maximization (EM) algorithm (Dobin et al., 2013). Normalized counts were analyzed for differential expression with the gene-specific analysis (GSA) method based on STAR default alignment. *A priori* criteria for differential expression were a false discovery rate (FDR) < 0.05 and > 2X difference in expression. Alignment was also performed with chimeric and 2-pass modes. Chimeric mode allows for detection of fusion alignments in addition to normal mapping whereas 2-pass mode enhances novel junction discovery.

To validate RNA-Seq data, QRT-PCR and Sanger sequencing were performed using primers located in exon 4, intron 4, exon 5, intron 5, and exon 6 (Table S1). Details regarding PCR conditions for *Ciz1* are provided in previous work from our laboratory (Xiao et al., 2016a).

Immunoprecipitation

The cerebellum and cerebral cortex were dissected from the brains of adult (3-month-old) *Ciz1*$^{+/+}$, *Ciz1*$^{-/-}$ and *Ciz1*$^{\Delta E5/\Delta E5}$ mice. Tissues were lysed with ice-cold IP lysis buffer from the Pierce™ Classic Magnetic IP/Co-IP kit (ThermoFisher Scientific) containing Halt™ protease and phosphatase inhibitor cocktail (ThermoFisher Scientific) using a Teflon glass homogenizer. Lysed samples were microcentrifuged for 15 min at 14,000 rpm and the collected supernatants were pre-cleaned with protein A/G magnetic beads for 3 to 4 hrs at 4 °C using a magnetic separation rack. Using 4 μg of mouse anti-CIZ1 antibody (ab172442, Abcam, Cambridge, MA, USA), total protein (500 μg) was immunoprecipitated overnight at 4 °C with constant rocking. Pull down was completed the next morning with 25 μL of protein A/G magnetic beads for 4 to 6 hrs at 4 °C. Beads were then washed 4X with ice-cold IP lysis buffer and bound proteins were eluted in 2X SDS sample buffer. For blotting with a BioRad (Berkeley, CA, USA) wet transfer system, proteins were separated by SDS-PAGE (4–12% Bis-Tris gels) and transferred to PVDF membranes. Subsequently, membranes were blocked for 2 hr in 5% non-fat dry milk and incubated overnight with mouse anti-CIZ1 primary antibody (Xiao et al., 2016b)(1:10,000; ab172442, Abcam) in phosphate-buffered saline with Tween 20 (PBST) containing 5% non-fat dry milk. Membranes were washed 3X with PBST for 15 min and then incubated with horseradish peroxidase-conjugated goat anti-mouse secondary antibody (Jackson ImmunoResearch Laboratories, West Grove, PA) for 1 hr with constant rocking at room temperature. Signal was detected using enhanced chemiluminescence (Amersham, Pittsburgh, PA).

Bioinformatics

NNSPLICE 0.9 (www.fruitfly.org/seq_tools/splice.html) (Reese et al., 1997) and NetGene2 (www.cbs.dtu.dk/services/NetGene2/) (Brunak et al., 1991) were used to predict 5’ and 3’ splice sites within *Ciz1*. Splice site scores range from 0 to 1. Higher scores are associated with greater probability of either a donor (5’) or acceptor (3’) site.

UniProt (www.uniprot.org), National Center for Biotechnology Information (www.ncbi.nlm.nih.gov/protein/), and Clustal Omega pairwise alignment of human and mouse CIZ1 were used to identify functional domains and sites of possible post-translational modifications. Phosphorylation sites within the region encoded by exon 5 were predicted with NetPhos 3.1 (www.cbs.dtu.dk/services/NetPhos/) (Blom et al., 1999). Phosphorylation prediction scores range from 0 to 1 with scores greater than 0.5 indicating a positive prediction. ExPASy (web.expasy.org/translate) was used to translate *Ciz1* nucleotide sequences.

Cell Culture and irradiation

MEFs were isolated from *Ciz1*$^{+/+}$ and *Ciz1*$^{\Delta E5/\Delta E5}$ embryos (N = 3/genotype) at 12 to 14 days gestation and cultured in Dulbecco’s modified Eagle’s medium (DMEM), supplemented with 10% fetal bovine serum, 1% L-glutamine and 1% penicillin-streptomycin as described in a recent publication from our laboratory (Khan et al., 2018). Cells were plated on gelatin-coated T25 tissue culture flasks in an incubator at 37°C with 5% CO_2. After the fourth passage, MEFs were exposed to γ-radiation (20 Gy) using a ^{137}Cs source. Immediately after irradiation, cells were returned to the incubator for recovery.

DNA damage and the cell-cycle analyses

For assessment of DNA damage, cells were plated on poly-l-lysine-coated coverslips and fixed with 4% paraformaldehyde. After fixation, cells were washed twice with 1X phosphate-buffered saline (PBS) and permeabilized with 0.3% Triton X-100 for 15 min followed by blocking with 1% bovine serum albumin in PBS. Cells were incubated with rabbit anti-53BP1 (ab21083, Abcam) for 2 hrs at room temperature, rinsed and incubated with a fluorescently-tagged secondary antibody (Jackson ImmunoResearch Laboratories) for 1 hr and then washed 3X with PBS. Coverslips were mounted onto slides with medium containing DAPI (H-1200, Vector). Images were captured and 53BP1+ foci were counted under an epifluorescence microscope using a 63X objective by an investigator blinded to genotype and treatment. At least 100 cells per genotype were analyzed to calculate the percentage of 53BP1+ cells.

For cell-cycle analysis, cells were fixed with ice-chilled 70% ethanol for 1 hr at −20 ^{o}C. Fixed cells were then washed 3X with PBS followed by incubation with propidium iodide (PI) staining buffer (PBS with RNaseA 100 μg/mL and PI 50 μg/mL) for 30 min. After the incubation period, cells were analyzed by flow cytometry (YETI, Propel Labs; Fort Collins, CO, USA). The percentage of cells in each phase was quantified with ModFit LT™ software (Verity, Topsham, ME, USA).

Behavioral assessments

Adult (3-month-old) *Ciz*$^{+/\Delta E5}$ mice, *Ciz1*$^{\Delta E5/\Delta E5}$ mice and sex-matched *Ciz*$^{+/+}$ littermates were subjected to a battery of motor and behavioral examinations including grip strength, cross-maze, open-field activity, rotarod, vertical rope climbing, and the raised-beam task. DigiGait™ analysis was limited to *Ciz1*$^{\Delta E5/\Delta E5}$ mice and sex-matched *Ciz*$^{+/+}$ littermates. Mice were weighed weekly and routinely observed for evidence of dystonia or other involuntary movements during open-field activity and routine handling. Sensorimotor and behavioral methods used in this study have previously been described in detail (Xiao et al., 2016a, Xiao et al., 2017, Toro et al., 2018, Khan et al., 2018).

Statistics

Analysis of variance was used to determine the overall effect of genotype on parametric behavioral measures with post-hoc tests applied *a posteriori*. The Mann-Whitney test was used to determine the effects of genotype within sex for a non-parametric behavioral measure (slips on the raised beam task). Two-tailed *t*-tests were used to determine the effects of genotype on the percentages of cells with 53BP1 foci and percentages of cells in the G1, S and G2 phases of the cell cycle. An alpha (α) of 0.05 was chosen for statistical significance.

Results

RNA and protein expression

RNA expression data generated with QRT-PCR was normalized to *Ciz1*$^{+/+}$ liver (Fig. 1, Table S2). Similar to our previous findings, total *Ciz1* expression was found to be highest in the cerebellum (Xiao et al., 2016a). *Ciz1* expression was normal in homozygous exon 5-

floxed mice (*Ciz1*$^{tm1Homy/tm1Homy}$). With primers placed in exons 5 and 6 (Primers 1), *Ciz1* expression was reduced by approximately 20 to 50% in *Ciz*$^{+/\Delta E5}$ mice, and eliminated in *Ciz1*$^{\Delta E5/\Delta E5}$ mice generated via crosses to both Sox2-cre and Hs-cre1 mice (Fig. 1, Table S2). In contrast, *Ciz1* expression levels were normal with primers placed in exons 11 and 12 (Primers 2).

RNA-Seq showed that *Ciz1*$^{\Delta E5/\Delta E5}$ mice express all *Ciz1* exons at near *Ciz*$^{+/+}$ levels with the exception of exon 5 (Fig. 2). A small number of non-*Ciz1* transcripts showed differential expression when compared to *Ciz1*$^{+/+}$ mouse cerebellum (Table S3). RNA-Seq reads mapped with STAR suggested the possible presence of multiple alternative transcripts derived, in part, from introns 3, 4 and 5 (Fig. 2, Fig. S1, and Fig. S2). Alignment and mapped reads were virtually identical with use of STAR's default, chimeric and 2-pass modes. *In silico* analyses with NNSPLICE and NetGene2 showed that the exon 4/intron 4 and intron 5/exon 6 donor and acceptor sites, respectively, are weak and multiple donor and acceptor sites are present in introns 4 and 5 (Table S4). However, analysis of individual raw reads did not expose novel intronic splice sites. Immunoprecipitation was compatible with QRT-PCR and RNA-Seq results and suggested the translation of one or more novel CIZ1 proteins of approximate WT size (Fig. 3). As seen from comparison of Figs. S3 and S4, deletion of exon 5 could be associated with use of an alternative translation start site and generation of a full-length protein, albeit smaller than CIZ1 isoform 1.

Deletion of exon 5 eliminates amino acids 120 to 196 from the N-terminal half of CIZ1 (Fig. 4). Although there are no well-defined functional domains in this region of relatively low complexity, there are three experimentally-validated (T138, T144, and T187) and three predicted (S177, T181, and S190) phosphorylation sites (Copeland et al., 2015) (Table S5).

DNA damage response and cell-cycle analysis in MEFs

To determine the contributions of CIZ1 to the DNA damage response, we subjected MEFs isolated from *Ciz1*$^{\Delta E5/\Delta E5}$ mice and *Ciz1*$^{+/+}$ littermates to γ-IR. At 24 hrs after IR (20 Gy), we assessed the persistence of DNA breaks using 53BP1 immunohistochemistry. In comparison to MEFs derived from *Ciz1*$^{-/-}$ embryos (Khan et al., 2018), MEFs isolated from *Ciz1*$^{\Delta E5/\Delta E5}$ embryos did not exhibit evidence of increased sensitivity to γ-IR (Figs. 5A and B). In addition, *Ciz1*$^{\Delta E5/\Delta E5}$ MEFs did not show overt evidence of cell-cycle abnormalities before or after γ-IR (Fig. 5C).

Sensorimotor and behavioral analyses

Male and female *Ciz1*$^{\Delta E5/\Delta E5}$ mice were fertile and pups of all genotypes (*Ciz1*$^{+/+}$, *Ciz1*$^{\Delta E5/\Delta E5}$, *Ciz1*$^{+/\Delta E5}$) and both sexes were born at normal Mendelian ratios. There was no evidence of dystonia or other involuntary movements noted while mice were routinely observed in their home cages during open field behavior and while handling from the early postnatal period through 1.5 yrs of age. As shown in Tables 1, 2 and 3, and Fig. 6, there were no overall effects of genotype on weights, grip strength, dominant tube, cross maze scores, rope climbing, open-field activity, gait parameters, raised-beam task, or rotarod in 3-month-old mice.

Discussion

CIZ1 was first identified as a CDK2 inhibitor p21 (Cip1/Waf1) interacting protein in a yeast 2-hybrid study (Mitsui et al., 1999). More recent work has exposed numerous functions for CIZ1 in DNA replication, cell proliferation, cell-cycle regulation and the DNA damage response (Warder and Keherly, 2003, Coverley et al., 2005, den Hollander et al., 2006, Rahman et al., 2007, Copeland et al., 2010, Greaves et al., 2012, Copeland et al., 2015, Ridings-Figueroa et al., 2017). *CIZ1* variants are associated with a variety of cancers, Alzheimer disease, and dystonia (Dahmcke et al., 2008, Higgins et al., 2012a, Liu et al., 2015, Xiao et al., 2012, Zhou et al., 2018). Studies of CIZ1 in neural and extra-neural tissues would benefit from a mouse model with conditional potential. Accordingly, we acquired and characterized $Ciz1^{+/tm1Homy}$ for temporal and spatial control of CIZ1 expression. Herein, we provide robust evidence that the loxP sites surrounding exon 5 of *Ciz1* are functional in $Ciz1^{+/tm1Homy}$ mice but Cre-mediated deletion of exon 5 does not generate a null allele.

In previous work, $Ciz1^{tm1.1Homy/tm1.1Homy}$ mice were generated via crosses with germline Cre-expressing mice without prior removal of the intron 5 FRT-flanked neo cassette (Nishibe et al., 2013). Presumably, this was done to save time. Expression of *Ciz1* transcript was not assessed with QRT-PCR (Nishibe et al., 2013). Although a Northern blot is provided in their supplementary Fig. 1C, no information is provided on the region targeted by their probe (probe sequence) and they did not include an RNA ladder (Nishibe et al., 2013). Although retention of the neo cassette could have increased the possibility of generating a true null allele, MEFs from these mice did not show evidence of defects in cell cycle, growth or DNA damage response (Nishibe et al., 2013). Moreover, no motor or behavioral abnormalities were reported by Nishibe and colleagues (Nishibe et al., 2013). However, it should be emphasized that the *Ciz1* floxed mice described herein underwent FLP-mediated deletion of the FRT-flanked neo cassette prior to crosses with germline Cre-expressing mice.

$Ciz1^{tm1.1Homy/tm1.1Homy}$ mice did develop various types of leukemias by retroviral insertional mutagenesis and MEFs were sensitive to hydroxyurea-mediated replication stress and susceptible to oncogene-induced cellular transformation (Nishibe et al., 2013). Deletion of exon 5 does eliminate phosphorylation sites that could play an essential role in the DNA replication activity of CIZ1 (Coverley et al., 2005). Alternatively, translation of novel proteins could have contributed to the identified cellular phenotypic abnormalities through gain-of-function mechanisms. In this context, gain-of-function with the appearance of abnormally large CIZ1-immunoreactive nuclear foci was suggested as a possible pathogenic mechanism for the p.S264G variant identified in a large American pedigree with dystonia (Xiao et al., 2012).

Although exon 5 is clearly eliminated in $Ciz1^{\Delta E5/\Delta E5}$ mice, it is difficult to harmonize our RNA-Seq, QRT-PCR, immunoprecipitation and *in silico* analyses. In particular, RNA-Seq did not validate the potential intronic splice sites identified via *in silico* analysis as important contributors to $Ciz1^{\Delta E5/\Delta E5}$ mRNA. Moreover, we could not amplify full-length cDNA to corroborate the results of immunoprecipitation. Although speculative, it is possible that alternative translation start sites and/or variable inclusion of short coding sequences from

introns 3, 4 and 5 into mature mRNA contributed to translation of novel CIZ1 proteins of near WT molecular weight.

Our analyses are instructional with regards to initial characterization of models with presumed conditional potential and echo previous suggestions in the literature (Yang et al., 2009). First, gene expression should be rigorously characterized with QRT-PCR, Northern blotting, Western blots, immunohistochemistry, and, if necessary, RNA-Seq. The importance of analyzing transcripts and protein from conditional knockout alleles was previously described for farnesyltransferase and β1 integrin alleles, respectively (Yang et al., 2009, Turlo et al., 2010). Second, *in silico* tools should be used to explore for cryptic splice sites in flanking introns, characterize splice sites at nearby intron-exon boundaries and alternative translation start sites. Third, intronic cassettes should be removed prior to Cre-mediated exonic excision. The neomycin resistance coding sequence and its promoter can have unintended consequences on the targeted gene and, occasionally, nearby genes (Pham et al., 1996).

In conclusion, *Ciz1* $^{\text{tm1.1Homy/tm1.1Homy}}$ mice show loss of *Ciz1* exon 5 but are neurologically normal and express alternative transcripts (*Ciz1*$^{\Delta E5/\Delta E5}$ mice) that are translated into one or more novel proteins of approximate wild-type size. Therefore, *Ciz1* $^{\text{tm1.1Homy/tm1.1Homy}}$ mice (*Ciz1*$^{\Delta E5/\Delta E5}$) lose residues encoded by exon 5 which may be essential for certain aspects of CIZ1 biology including its role in DNA replication, but CIZ1 may also gain function from chimeric protein sequences. *Ciz1* $^{\text{tm1.1Homy/tm1.1Homy}}$ mice are not a valid null (KO) model.

Supplementary Material

Refer to Web version on PubMed Central for supplementary material.

Acknowledgments

This study was supported by the Neuroscience Institute at the University of Tennessee Health Science Center, Dorothy/Daniel Gerwin Parkinson's Research Fund, Department of Defense grant W81XWH-17-1-0062 and National Institutes of Health (NIH) grants R01 NS082296, R01 NS069936, R21 GM118962, and R56 NS094965.

References

AINSCOUGH JF, RAHMAN FA, SERCOMBE H, SEDO A, GERLACH B & COVERLEY D 2007 C-terminal domains deliver the DNA replication factor Ciz1 to the nuclear matrix. J Cell Sci, 120, 115–24. [PubMed: 17182902]

BLOM N, GAMMELTOFT S & BRUNAK S 1999 Sequence and structure-based prediction of eukaryotic protein phosphorylation sites. J Mol Biol, 294, 1351–62. [PubMed: 10600390]

BRUNAK S, ENGELBRECHT J & KNUDSEN S 1991 Prediction of human mRNA donor and acceptor sites from the DNA sequence. J Mol Biol, 220, 49–65. [PubMed: 2067018]

COPELAND NA, SERCOMBE HE, AINSCOUGH JF & COVERLEY D 2010 Ciz1 cooperates with cyclin-A-CDK2 to activate mammalian DNA replication in vitro. J Cell Sci, 123, 1108–15. [PubMed: 20215406]

COPELAND NA, SERCOMBE HE, WILSON RH & COVERLEY D 2015 Cyclin-A-CDK2-mediated phosphorylation of CIZ1 blocks replisome formation and initiation of mammalian DNA replication. J Cell Sci, 128, 1518–27. [PubMed: 25736292]

COVERLEY D, MARR J & AINSCOUGH J 2005 Ciz1 promotes mammalian DNA replication. J Cell Sci, 118, 101–12. [PubMed: 15585571]

DAHMCKE CM, BUCHMANN-MOLLER S, JENSEN NA & MITCHELMORE C 2008 Altered splicing in exon 8 of the DNA replication factor CIZ1 affects subnuclear distribution and is associated with Alzheimer's disease. Mol Cell Neurosci, 38, 589–94. [PubMed: 18583151]

DEN HOLLANDER P, RAYALA SK, COVERLEY D & KUMAR R 2006 Ciz1, a Novel DNA-binding coactivator of the estrogen receptor alpha, confers hypersensitivity to estrogen action. Cancer Res, 66, 11021–9. [PubMed: 17108141]

DIETRICH P, DRAGATSIS I, XUAN S, ZEITLIN S & EFSTRATIADIS A 2000 Conditional mutagenesis in mice with heat shock promoter-driven cre transgenes. Mamm Genome, 11, 196–205. [PubMed: 10723724]

DOBIN A, DAVIS CA, SCHLESINGER F, DRENKOW J, ZALESKI C, JHA S, BATUT P, CHAISSON M & GINGERAS TR 2013 STAR: ultrafast universal RNA-seq aligner. Bioinformatics, 29, 15–21. [PubMed: 23104886]

GREAVES EA, COPELAND NA, COVERLEY D & AINSCOUGH JF 2012 Cancer-associated variant expression and interaction of CIZ1 with cyclin A1 in differentiating male germ cells. J Cell Sci, 125, 2466–77. [PubMed: 22366453]

HIGGINS G, COOK H, ROPER K, MUNCKLEY J, WATSON I, BLACKHALL F, ROM W, PASS H, AINSCOUGH J & COVERLEY DA 2012a The nuclear matrix anchor domain of the DNA replication factor Ciz1 is commonly disrupted in tumours and is a circulating biomarker for lung cancer. Cancer Research, 72.

HIGGINS G, ROPER KM, WATSON IJ, BLACKHALL FH, ROM WN, PASS HI, AINSCOUGH JF & COVERLEY D 2012b Variant Ciz1 is a circulating biomarker for early-stage lung cancer. Proc Natl Acad Sci U S A, 109, E3128–35. [PubMed: 23074256]

JUDEX M, NEUMANN E, LECHNER S, DIETMAIER W, BALLHORN W, GRIFKA J, GAY S, SCHOLMERICH J, KULLMANN F & MULLER-LADNER U 2003 Laser-mediated microdissection facilitates analysis of area-specific gene expression in rheumatoid synovium. Arthritis Rheum, 48, 97–102. [PubMed: 12528109]

KHAN MM, XIAO J, PATEL D & LEDOUX MS 2018 DNA damage and neurodegenerative phenotypes in aged Ciz1 null mice. Neurobiol Aging, 62, 180–190. [PubMed: 29154038]

LIU T, REN X, LI L, YIN L, LIANG K, YU H, REN H, ZHOU W, JING H & KONG C 2015 Ciz1 promotes tumorigenicity of prostate carcinoma cells. Front Biosci (Landmark Ed), 20, 705–15. [PubMed: 25553473]

MITSUI K, MATSUMOTO A, OHTSUKA S, OHTSUBO M & YOSHIMURA A 1999 Cloning and characterization of a novel p21(Cip1/Waf1)-interacting zinc finger protein, ciz1. Biochem Biophys Res Commun, 264, 457–64. [PubMed: 10529385]

NISHIBE R, WATANABE W, UEDA T, YAMASAKI N, KOLLER R, WOLFF L, HONDA Z, OHTSUBO M & HONDA H 2013 CIZ1, a p21Cip1/Waf1-interacting protein, functions as a tumor suppressor in vivo. FEBS Lett, 587, 1529–35. [PubMed: 23583447]

PHAM CT, MACIVOR DM, HUG BA, HEUSEL JW & LEY TJ 1996 Long-range disruption of gene expression by a selectable marker cassette. Proc Natl Acad Sci U S A, 93, 13090–5. [PubMed: 8917549]

RAHMAN F, AINSCOUGH JF, COPELAND N & COVERLEY D 2007 Cancer-associated missplicing of exon 4 influences the subnuclear distribution of the DNA replication factor CIZ1. Hum Mutat, 28, 993–1004. [PubMed: 17508423]

REESE MG, EECKMAN FH, KULP D & HAUSSLER D 1997 Improved splice site detection in Genie. J Comput Biol, 4, 311–23. [PubMed: 9278062]

RIDINGS-FIGUEROA R, STEWART ER, NESTEROVA TB, COKER H, PINTACUDA G, GODWIN J, WILSON R, HASLAM A, LILLEY F, RUIGROK R, BAGEGHNI SA, ALBADRANI G, MANSFIELD W, ROULSON JA, BROCKDORFF N, AINSCOUGH JFX & COVERLEY D 2017 The nuclear matrix protein CIZ1 facilitates localization of Xist RNA to the inactive X-chromosome territory. Genes Dev, 31, 876–888. [PubMed: 28546514]

TORO C, HORI RT, MALICDAN MCV, TIFFT CJ, GOLDSTEIN A, GAHL WA, ADAMS DR, HARPER F, WOLFE LA, XIAO J, KHAN MM, TIAN J, HOPE KA, REITER LT, TREMBLAY

MG, MOSS T, FRANKS AL, BALAK C, GROUP CRR & LEDOUX MS 2018 A recurrent de novo missense mutation in UBTF causes developmental neuroregression. Hum Mol Genet

TURLO KA, GALLAHER SD, VORA R, LASKI FA & IRUELA-ARISPE ML 2010 When Cre-mediated recombination in mice does not result in protein loss. Genetics, 186, 959–67. [PubMed: 20813881]

WARDER DE & KEHERLY MJ 2003 Ciz1, Cip1 interacting zinc finger protein 1 binds the consensus DNA sequence ARYSR(0–2)YYAC. J Biomed Sci, 10, 406–17. [PubMed: 12824700]

WU J, LEI L, GU D, LIU H & WANG S 2015 CIZ1 is upregulated in hepatocellular carcinoma and promotes the growth and migration of the cancer cells. Tumour Biol

XIAO J, UITTI RJ, ZHAO Y, VEMULA SR, PERLMUTTER JS, WSZOLEK ZK, MARAGANORE DM, AUBURGER G, LEUBE B, LEHNHOFF K & LEDOUX MS 2012 Mutations in CIZ1 cause adult onset primary cervical dystonia. Ann Neurol, 71, 458–69. [PubMed: 22447717]

XIAO J, VEMULA SR, XUE Y, KHAN MM, CARLISLE FA, WAITE AJ, BLAKE DJ, DRAGATSIS I, ZHAO Y & LEDOUX MS 2017 Role of major and brain-specific Sgce isoforms in the pathogenesis of myoclonus-dystonia syndrome. Neurobiol Dis, 98, 52–65. [PubMed: 27890709]

XIAO J, VEMULA SR, XUE Y, KHAN MM, KURUVILLA KP, MARQUEZ-LONA EM, COBB MR & LEDOUX MS 2016a Motor phenotypes and molecular networks associated with germline deficiency of Ciz1. Exp Neurol, 283, 110–120. [PubMed: 27163549]

XIAO J, VEMULA SR, XUE Y, KHAN MM, KURUVILLA KP, MARQUEZ-LONA EM, COBB MR & LEDOUX MS 2016b Motor phenotypes and molecular networks associated with germline deficiency of Ciz1. Exp Neurol, 283, 110–20. [PubMed: 27163549]

YANG SH, BERGO MO, FARBER E, QIAO X, FONG LG & YOUNG SG 2009 Caution! Analyze transcripts from conditional knockout alleles. Transgenic Res, 18, 483–9. [PubMed: 19093225]

YIN J, WANG C, TANG X, SUN H, SHAO Q, YANG X & QU X 2013 CIZ1 regulates the proliferation, cycle distribution and colony formation of RKO human colorectal cancer cells. Mol Med Rep, 8, 1630–4. [PubMed: 24126760]

ZHOU X, LIU Q, WADA Y, LIAO L & LIU J 2018 CDKN1A-interacting zinc finger protein 1 is a novel biomarker for lung squamous cell carcinoma. Oncol Lett, 15, 183–188. [PubMed: 29285191]

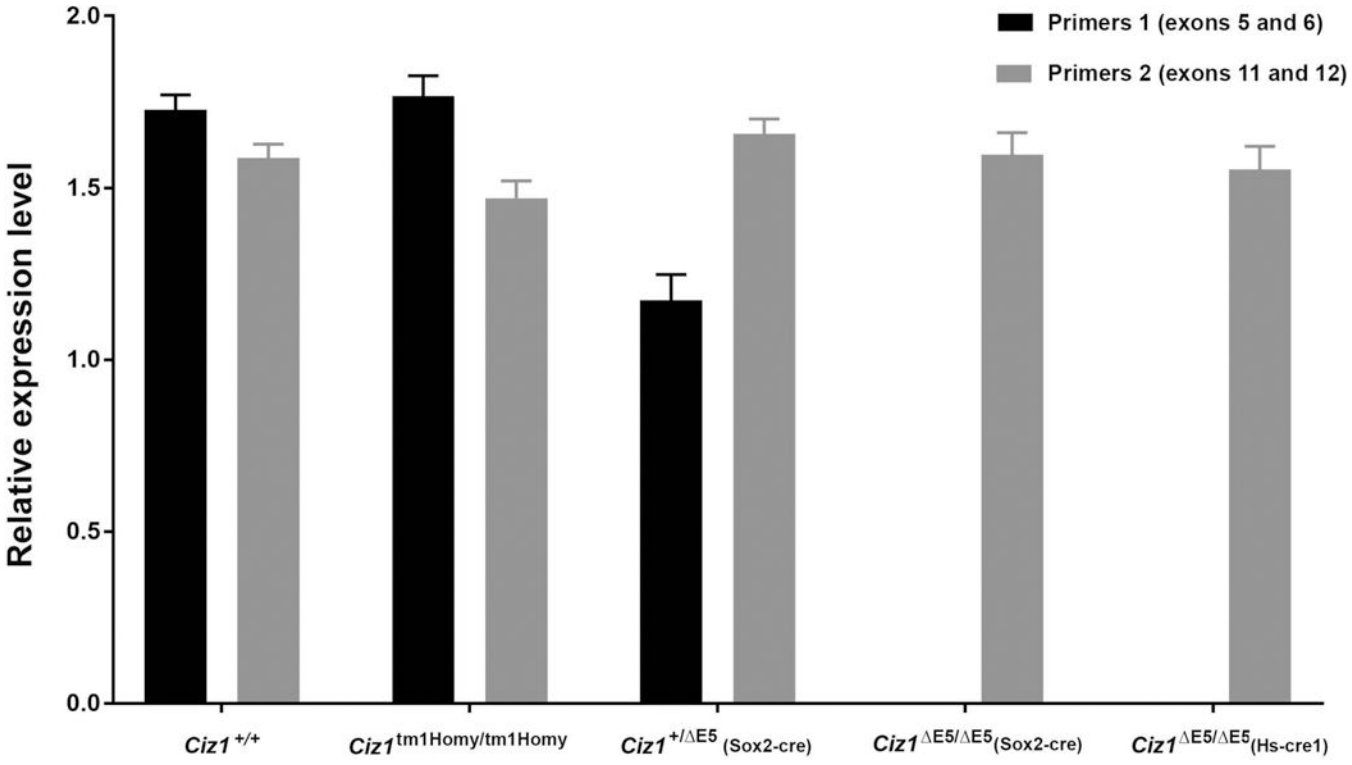

Fig. 1.
Comparative expression of *Ciz1* transcripts in the cerebellum with QRT-PCR.

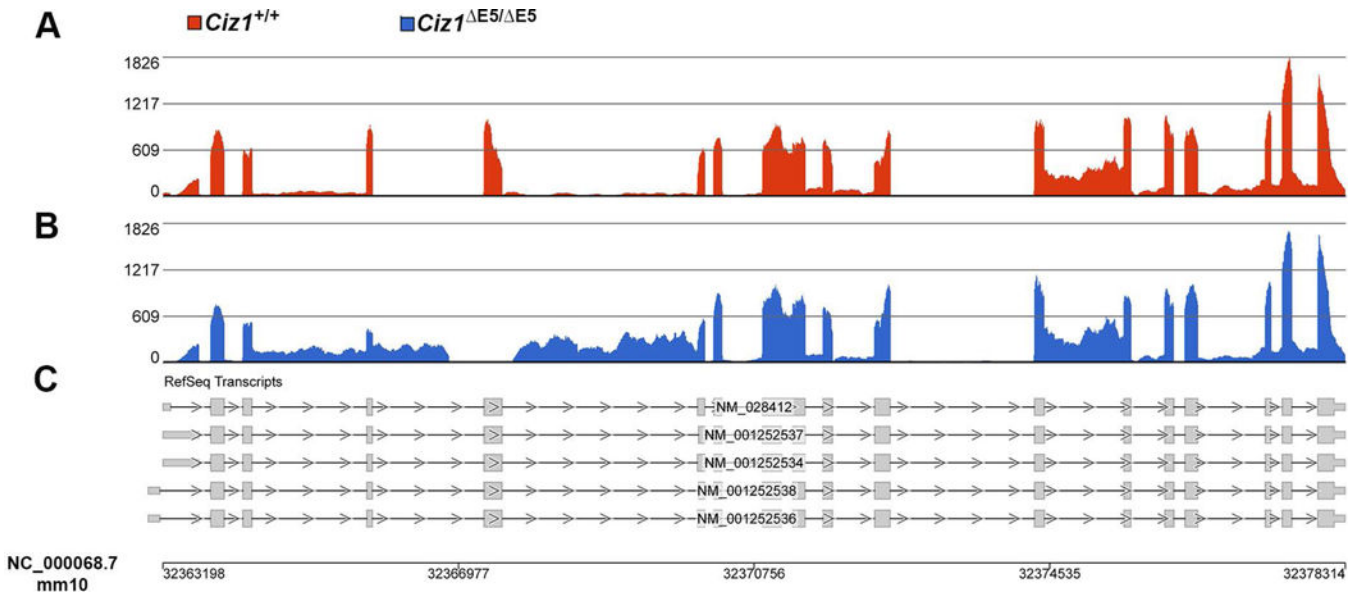

Fig. 2.

Expression of *Ciz1* transcripts. RNA-Seq of (A) *Ciz1*$^{+/+}$ (red) and (B) *Ciz1*$^{\Delta E5/\Delta E5}$ (blue) mice showing absence of exon 5 expression in *Ciz1*$^{\Delta E5/\Delta E5}$ (blue) mice. Read numbers and genomic coordinates are represented on the vertical and horizontal axes, respectively. (C) Mouse *Ciz1* RefSeq genes.

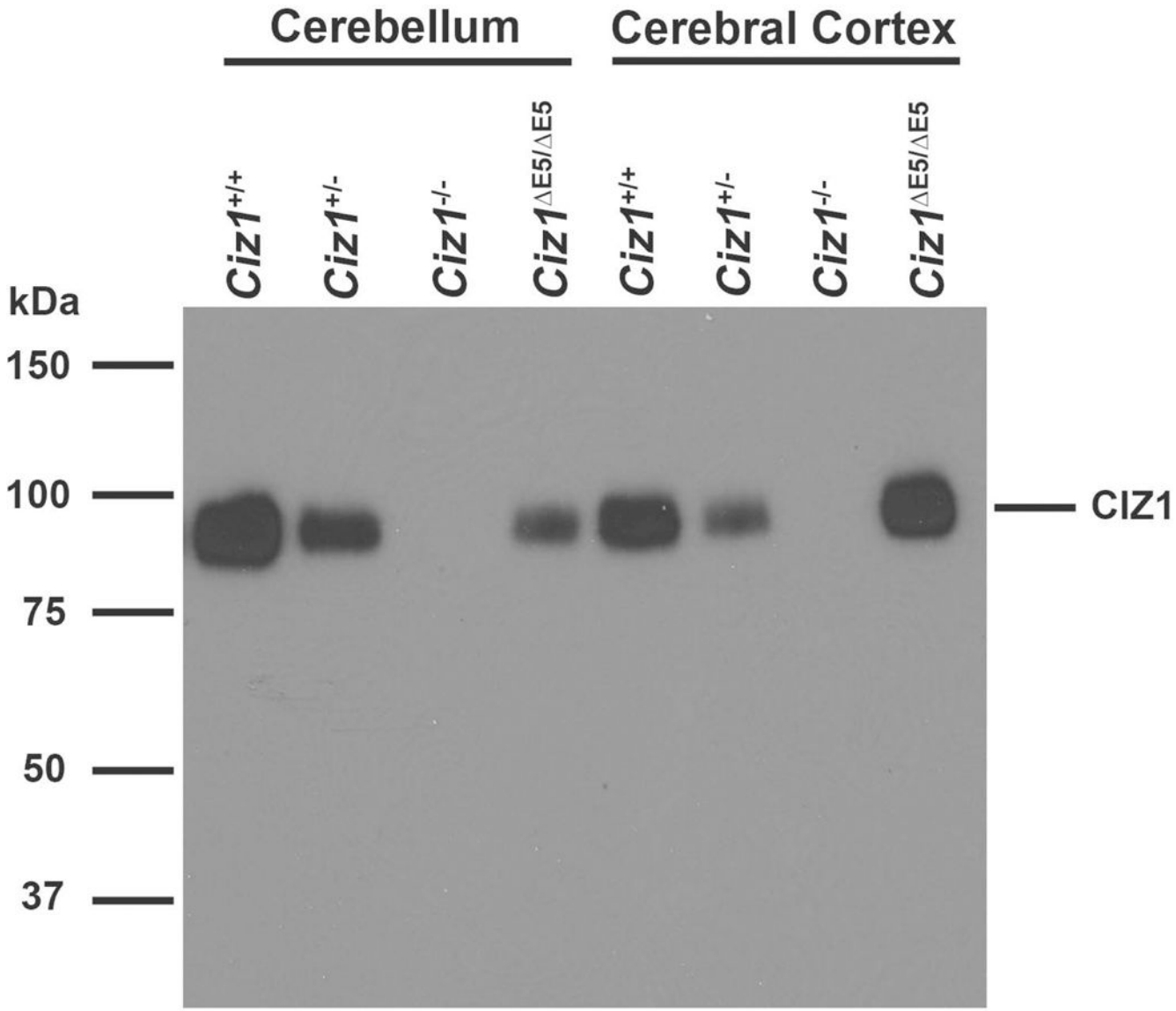

Fig. 3.

Blotting of immunoprecipitated lysates from cerebellum and cerebral cortex. *Ciz1*$^{+/+}$ mouse; *Ciz1*$^{+/-}$, gene-trap heterozygote mouse; *Ciz1*$^{-/-}$, gene-trap homozygote mouse; *Ciz1*$^{\Delta E5/\Delta E5}$ mouse.

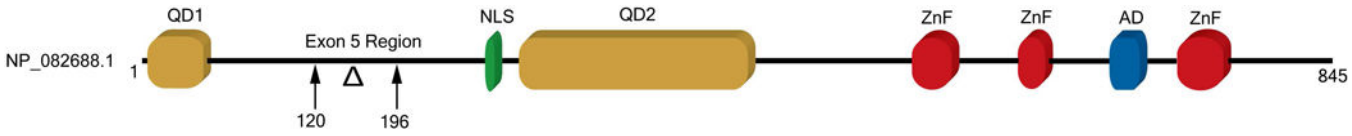

Fig. 4.

Mouse CIZ1. QD1, glutamine-rich domain 1; NLS, nuclear localization signal; QD2, glutamine-rich domain 2; ZnF, zinc finger; AD, glutamic acid-rich acidic domain. Region encoded by exon 5 deletion (Δ) denoted with arrows on the diagram.

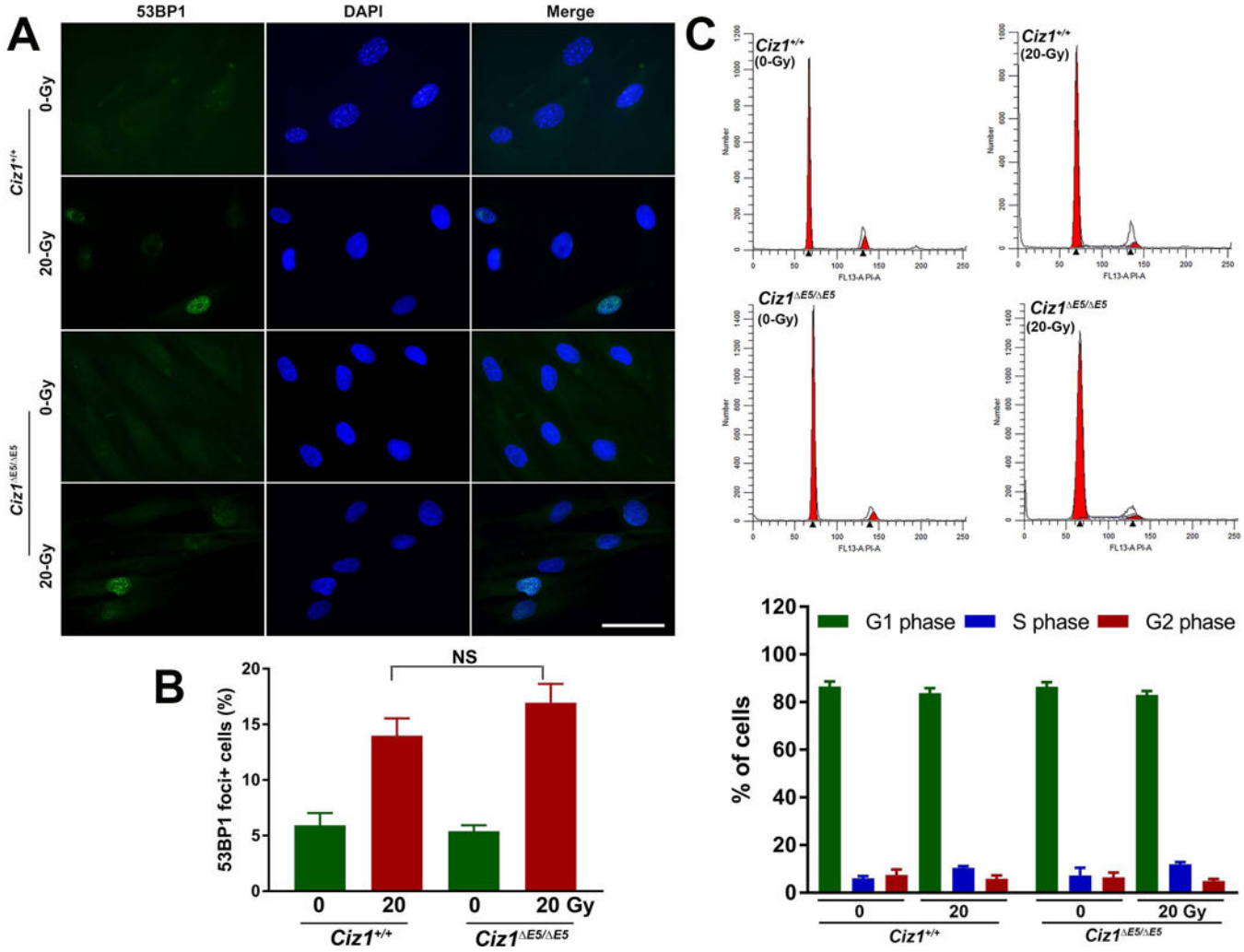

Fig. 5.

DNA damage and cell-cycle progression in irradiated MEFs derived from *Ciz1*$^{\Delta E5/\Delta E5}$ mice and *Ciz1*$^{+/+}$ littermates. MEFs isolated from *Ciz1*$^{+/+}$ and *Ciz1*$^{\Delta E5/\Delta E5}$ embryos were subjected to 20 Gy γ-irradiation (IR). At 24 h after γ-IR, DNA damage and cell-cycle were assessed with 53BP1-immunohistochemistry (A and B), and flow cytometry (C). Untreated MEFs from *Ciz1*$^{+/+}$ and *Ciz1*$^{\Delta E5/\Delta E5}$ mice showed negligible expression of 53BP1. Similarly, there was no significant difference in the percentage of cells with 53BP1+ foci between irradiated MEFs from *Ciz1*$^{+/+}$ and *Ciz1*$^{\Delta E5/\Delta E5}$ mice. Values are expressed as means ± SEM. Scale bar for A, 50 μm.

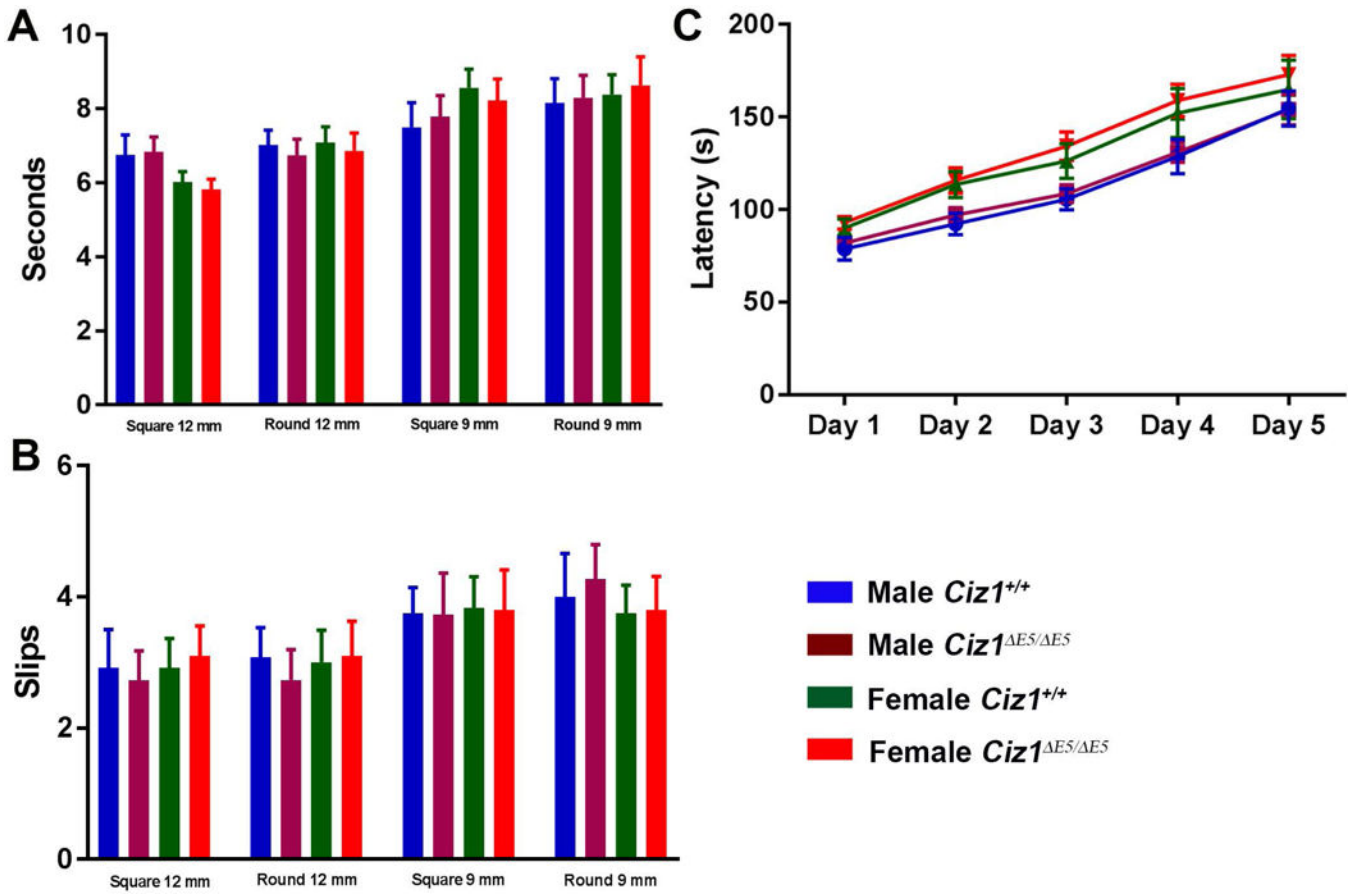

Fig. 6.

Performance of *Ciz1*$^{\Delta E5/\Delta E5}$ mice and their *Ciz1*$^{+/+}$ littermates on the raised beam tasks (A and B) and accelerating rotarod (C). Beam traversal times (A) and slips (B) were recorded for 4 different beams. Values are expressed as means ± SEM.

Table 1.

Weight, grip strength, tube dominance, cross maze scores, and rope climbing in 3-month-old mice.

Gender	Genotypes	Weight (g)	Grip strength (g)	Grip strength /weight	Dominance tube	Cross maze score (%)	Rope climbing (s)	Rope climbing/weight
Male	*Ciz1*$^{+/+}$ (n=12)	30.9 ± 0.4	32.9 ± 0.6	1.07 ± 0.03	NA	30.9 ± 2.4	5.8 ± 0.4	0.19 ± 0.01
	Ciz1$^{+/\Delta E5}$ (n=12)	30.0 ± 0.4	31.9 ± 0.4	1.07 ± 0.02	NA	30.0 ± 2.0	4.9 ± 0.4	0.16 ± 0.01
	Ciz1$^{\Delta E5/\Delta E5}$ (n=11)	30.1 ± 0.3	32.1 ± 0.3	1.06 ± 0.02	51%	29.7 ± 1.5	4.8 ± 0.4	0.16 ± 0.01
Female	*Ciz1*$^{+/+}$ (n=12)	21.9 ± 0.3	25.2 ± 0.5	1.15 ± 0.03	NA	31.9 ± 2.0	4.9 ± 0.4	0.23 ± 0.02
	Ciz1$^{+/\Delta E5}$ (n=11)	21.7 ± 0.3	25.5 ± 0.4	1.18 ± 0.02	NA	29.1 ± 2.1	4.9 ± 0.3	0.22 ± 0.02
	Ciz1$^{\Delta E5/\Delta E5}$ (n=10)	21.3 ± 0.2	25.3 ± 0.5	1.19 ± 0.03	54%	32.7 ± 1.4	4.8 ± 0.4	0.23 ± 0.02

Values are means ± SEM except for dominance tube. NA, not applicable.

Table 2.

Open field activity.

Gender	Genotypes	Distance Traveled (cm)	Ambulatory Count	Stereotypic Count	Vertical Count	Jump Count	Average Velocity (cm/s)	Ambulatory Episodes
Male	*Ciz1*$^{+/+}$ (n=12)	1871.6 ± 67.6	893.0 ± 41.9	2741.7 ± 114.3	200.5 ± 15.0	57.1 ± 3.4	38.5 ± 2.0	84.9 ± 3.8
	Ciz1$^{+/\Delta E5}$ (n=12)	1952.0 ± 42.2	904.6 ± 27.7	2795.0 ± 77.2	228.5 ± 13.1	54.9 ± 3.1	40.6 ± 2.3	91.2 ± 3.8
	Ciz1$^{\Delta E5/\Delta E5}$ (n=11)	1995.8 ± 75.0	965.3 ± 44.4	2727.5 ± 66.2	226.7 ± 10.4	52.1 ± 4.0	40.0 ± 2.3	93.8 ± 6.1
Female	*Ciz1*$^{+/+}$ (n=12)	2445.5 ± 68.4	1279.6 ± 41.0	2537.2 ± 61.2	130.8 ± 10.4	41.2 ± 3.8	41.9 ± 2.8	113.2 ± 5.6
	Ciz1$^{+/\Delta E5}$ (n=11)	2385.5 ± 54.2	1219.9 ± 35.8	2464.7 ± 90.7	122.8 ± 4.4	40.1 ± 2.8	41.0 ± 2.7	107.6 ± 1.9
	Ciz1$^{\Delta E5/\Delta E5}$ (n=10)	2347.4 ± 42.0	1209.7 ± 45.0	2426.5 ± 77.7	120.7 ± 15.5	37.4 ± 5.7	43.2 ± 2.8	102.8 ± 5.0

Values are means ± SEM. Ambulatory count, the total number of X + Y photo beam breaks while in ambulatory movement status. Stereotypic count, any partial-body movements that occur within the ambulatory box such as grooming, head-weaving or scratching. Vertical count, number of periods of continuous Z photo beam breaks. Jump count, the number of times that the mouse leaves the photo beam array for a period of time. Ambulatory episodes, the number of times the mouse has started moving after the resting delay has expired.

Table 3.

DigiGait™ analyses.

Gender, Genotype (numbers)	Propel (s)		Stride length (cm)		Stride Frequency (steps/s)		Stance width (cm)		Step angle (deg)		Paw Area (cm^2)	
	Fore	Hind	Fore	Hind	Fore	Hind	Fore	Hind	Fore	Hind	Fore	Hind
M, WT (n=12)	0.123 ±0.004	0.181 ±0.004	6.82 ±0.18	7.09 ±0.13	3.09 ±0.05	2.95 ±0.05	1.77 ±0.04	2.77 ±0.07	68.91 ±2.49	57.40 ±2.40	0.230 ±0.006	0.456 ±0.010
M, *Ciz1*$^{\Delta E5/\Delta E5}$ (n=11)	0.124 ±0.003	0.180 ±0.004	6.61 ±0.08	7.15 ±0.12	3.13 ±0.04	3.00 ±0.04	1.69 ±0.03	2.71 ±0.06	66.39 ±2.25	58.50 ±1.50	0.222 ±0.011	0.443 ±0.015
F, WT (n=12)	0.116 ±0.004	0.165 ±0.004	6.33 ±0.15	6.59 ±0.13	3.31 ±0.07	3.14 ±0.07	1.53 ±0.04	2.34 ±0.03	68.39 ±1.62	65.08 ±1.44	0.204 ±0.006	0.378 ±0.008
F, *Ciz1*$^{\Delta E5/\Delta E5}$ (n=10)	0.106 ±0.006	0.162 ±0.002	6.23 ±0.08	6.54 ±0.07	3.46 ±0.11	3.23 ±0.06	1.49 ±0.04	2.33 ±0.05	66.48 ±1.39	63.75 ±1.63	0.215 ±0.009	0.392 ±0.015

Values are means ± SEM.